Bulk refractive-index sensitivities of the THz-range plasmon resonances on a micro-size graphene strip

2016 J. Phys. D: Appl. Phys. 49 055105

(http://iopscience.iop.org/0022-3727/49/5/055105)

IOP Publishing Journal of Physics D: Applied Physics

J. Phys. D: Appl. Phys. **49** (2016) 055105 (8pp) doi:10.1088/0022-3727/49/5/055105

Bulk refractive-index sensitivities of the THz-range plasmon resonances on a micro-size graphene strip

Olga V Shapoval and Alexander I Nosich

Laboratory of Micro & Nano Optics, Institute of Radio-Physics & Electronics NASU, Kharkiv 61085, Ukraine

E-mail: olga.v.shapoval@gmail.com

Received 26 August 2015, revised 3 December 2015
Accepted for publication 8 December 2015
Published 12 January 2016

Abstract

We studied numerically the potential use of a micro-size graphene strip as a surface plasmon (SP) resonance-based bulk refractive-index sensor in the THz frequency regime. Our accurate computational instrument was an in-house algorithm based on integral equations (IEs) and Nystrom discretization. The refractive-index sensitivities and figure-of-merit (FOM) values of the associated plasmon resonances were calculated. It was found that the primary plasmon mode P_1 is more sensitive to the refractive-index changes than plasmons of higher orders, although the latter demonstrated much larger FOM values explained by the higher Q-factors. The FOM values of the higher-order resonances on a graphene strip in the THz range are at a level similar to the FOM values of the localized SP resonances on a noble-metal strip in the optical range.

Keywords: micro-size strips, graphene, surface plasmons, singular integral equations, Nystrom-type discretization, refractive-index sensitivities

(Some figures may appear in colour only in the online journal)

1. Introduction

Graphene is attractive as a non-conventional material for creating fundamentally novel tunable nanoelectrical, nano-mechanical, and nanochemical devices [1–12]. It is also known for the high electromagnetic field localization near to its surface that offers new applications in antennas and absorbers. Moreover, thanks to the inductive nature of graphene's surface impedance, it is able to support the natural surface plasmon (SP) wave, which is a transverse-magnetic wave caused by the collective oscillations of surface charges. As a result, intensive SP resonances exist on the patterned (i.e. finite) graphene samples, shaped as SP standing waves created by the reflections of the above-mentioned natural SP wave from the sample edges. Then the size of the graphene sample determines the range of the SP resonance frequencies: it varies from the infra-red for the nano-size samples to the THz range for the micro-scale ones.

SP resonances on graphene nano-objects present a remarkable alternative to conventionally used noble-metal nanoparticles in the optical range [13–15] in the context of the design and development of high-performance sensors of small changes in the environment refractive index. Here, the important advantages of graphene are its electronic and mechanical properties such as high electron conductivity combined with exceptional durability. One of the most promising features of graphene as compared with metals is the opportunity to alter its conductivity by applying an external electrostatic biasing field, which modifies graphene's chemical potential. This can be easily realized in practice. For instance, one can use a thin polysilicon layer as a dielectric substrate supporting the graphene, and apply a dc bias, as was suggested in [1, 2, 7].

Still, one can find that the analysis of graphene strips as sensors has so far been concentrated on the modeling of nano-size strips analyzed as visible-range and infra-red sensors. Unfortunately, these simulations may be not sufficiently correct, because it has been experimentally demonstrated [16] that the edge effects in graphene conductivity are important in structures with dimensions smaller than 100 nm. Only for considerably wider strips can one disregard the edge effects

in the conductivity and use the electron conductivity model developed for infinite graphene sheets. These wider strips have their SP resonances at the sub-THz and THz frequencies, and their sensing characteristics have not been modeled in detail so far.

Additional motivation to move the sensing to the THz range can be found in the fact that this range is very actively investigated and developed today. This promises efficient all-terahertz sources, circuits, and systems in the near future.

In this paper we presented a numerical analysis of the SP resonances on a micro-size graphene strip and the corresponding sensing properties with respect to the host medium refractive-index changes in the THz range. We also derived advanced analytical expressions that yield the sensitivity and figure-of-merit (FOM) values for a graphene strip with an accuracy acceptable for quick practical evaluations. Although graphene strips are commonly placed on a substrate, we considered a strip suspended in a homogeneous medium. This enabled us to eliminate the effects of the substrate that need another focused study. Note also that suspended-graphene configurations are also realizable and are getting increasing attention [18, 19], apparently because the graphene conductivity can be degraded by the adjacent substrate.

We believe that our current analysis is important as providing the limit values of the sensitivities of the plasmon resonances. This is based on the well-established understanding that the 'surface sensitivity' of the resonances on a strip with a finite-thickness layer of the analyte is always smaller than the 'bulk sensitivity' and tends to the latter if the layer becomes thicker than the wavelength in material [17].

Throughout this paper, the time dependence was adopted as $\exp(-\mathrm{i}\omega t)$.

2. Essentials of numerical modeling

Our study of the bulk refractive-index sensitivities of the SP resonances of a micro-size graphene strip of width d (see figure 1(a)) in the THz frequency range was done using a widely accepted model of graphene conductivity and an advanced in-house numerical code based on the fast and *a priori* convergent solution to the associated singular integral equation (IE).

A graphene monolayer is a single-atom layer of graphite and hence can be viewed, in terms of the modeling, as a zero-thickness electrically conducting sheet even at frequencies as high as the optical range. Its electron conductivity $\sigma(\omega, \mu_c, \tau, T)$ depends on the angular frequency ω, temperature T, electron relaxation time τ, and chemical doping potential μ_c [1–8]. We used a model of graphene's conductivity known as Kubo's formalism, the details of which can be found in appendix A.

According to that model (see figure 1(b)), the conductivity in the THz range is a complex-valued function of the frequency. The unique property of graphene is that the associated surface impedance $Z(\omega) = 1/\sigma(\omega)$ is 'inductive', i.e. has a negative imaginary part if the time-dependence convention is adopted as $\exp(-i\omega t)$. As a result of this circumstance, a sheet of graphene can support traveling SP wave at THz frequencies

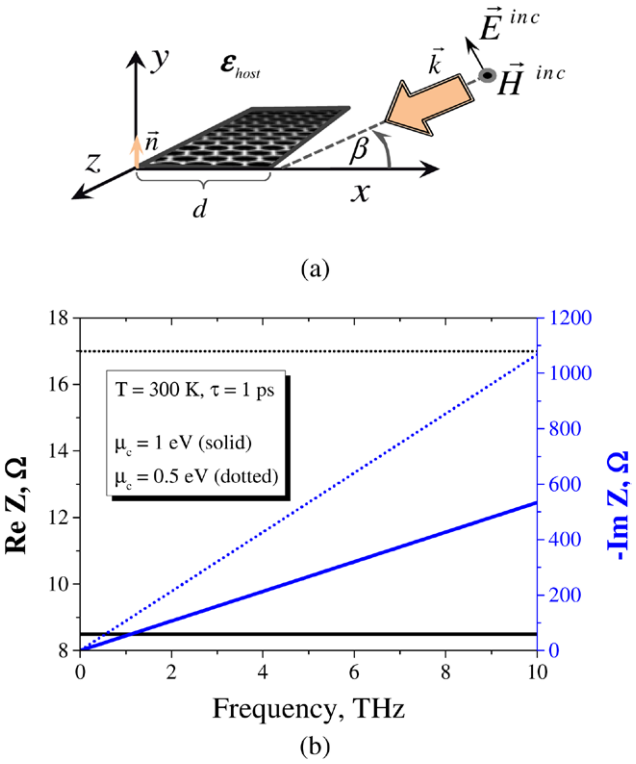

Figure 1. (a) Micro-size graphene strip illuminated by a plane wave, and (b) real and imaginary parts of the graphene impedance Z versus the frequency in the THz range.

that are two orders lower than for the noble metals. Note also that Z has a nearly constant real part controlled by the chemical potential, a nearly linearly varying imaginary part, and $|\mathrm{Im}\, Z(\omega)| \approx \mathrm{const} \cdot \omega \gg Z_0 \gg \mathrm{Re}\, Z(\omega)$ in the whole THz range, where $Z_0 = 120\pi\ \Omega$ is the free-space impedance.

A strip is an example of the patterned graphene; hence it displays pronounced resonances in the scattering and absorption of THz waves polarized orthogonally to the strip edge. Each resonance is caused by the corresponding standing-wave natural mode created by the reflections of the above-mentioned SP wave from the strip edges. These resonances were revealed in the papers [20, 21] and are well documented by now using a variety of approximate modeling methods, both on stand-alone graphene strips and on arrays of these strips [22–27].

For the proper positioning of the above-mentioned works it is necessary to emphasize that the numerical results of [20, 21] were obtained by an algorithm that was divergent (see the discussion of this divergence in [24, 25]). Practically speaking, this means that although the first 2–3 digits (and sometimes even fewer) of the numerical solution can be established correctly, the attempt to reduce the error by increasing the discretization order fails. It is still worth noting a certain mystery: in [20], the existence of so-called 'edge modes' in addition to SP modes was reported; however, in the analysis of the scattering by the grating of these strips no resonances on the edge modes were found in any of the papers [21–27].

A trusted and efficient instrument for the modeling of the scattering by graphene strips and the associated resonances with the desired accuracy can be based either on the Nystrom

discretization of the corresponding singular IE [23, 24] or on the analytical regularization of that IE [27]. In each case the convergence is guaranteed by the corresponding mathematical theorems. We used the former approach and code.

The associated IE is derived as follows. The scattered field function H_z must satisfy the Helmholtz equation in two dimensions (2D), the boundary conditions at the graphene strip, the edge condition, and the Sommerfeld radiation condition at infinity. The graphene strip is electromagnetically characterized [1, 2, 28, 29] with the aid of the following boundary condition with complex surface impedance Z, for the field components tangential (tg) at the top (+) and bottom (−) sides of the strip [28, 29]:

$$(1/2)[\vec{E}^{+}_{\rm tg}+\vec{E}^{-}_{\rm tg}]=Z\,\vec{n}\times[\vec{H}^{+}_{\rm tg}-\vec{H}^{-}_{\rm tg}],\quad \vec{E}^{+}_{\rm tg}=\vec{E}^{-}_{\rm tg}. \tag{1}$$

This pair of equations is easily identified as the so-called 'zero-thickness resistive-sheet' condition, which was introduced in the 1980s in the studies of the microwave-range scattering by thin dielectric and imperfect metal screens; see, for instance, the papers [30–33] and the further references therein.

Presenting the H_z-component of the scattered field as a double-layer potential we satisfy both the Helmholtz equation and the radiation condition. Then, using (1) and introducing the normalized coordinate $t=2x/d-1$, we obtain the equation fully equivalent to the original problem,

$$4(Z/Z_0)w(t_0)+\int_{-1}^{1} w(t)\frac{H_1^{(1)}(\kappa|t-t_0|)}{|t-t_0|}\,{\rm d}t=4\sin\,\beta{\rm e}^{-{\rm i}\kappa(t_0+1)\cos\beta} \tag{2}$$

for the unknown density function $w(t)=H_z^{+}(t)-H_z^{-}(t)$, which is the surface current induced on the graphene strip. Here, $\kappa=kd/2$ is the normalized frequency parameter, and $H_1^{(1)}(\bullet)$ is the Hankel function. Note that this IE is hyper-singular and should be understood in the sense of Hadamard's finite part. Hence, simple method-of-moments algorithms (found behind FEKO and other commercial software) based on the meshing of the strip contour and the use of local basis functions diverge since denser meshing does not lead to more accurate discrete approximation of the hyper-singular kernel. The same is true for the Fourier-expansion method (also called the Rigorous Coupled-Wave Algorithm) in the case of an array of strips.

Therefore, in [23, 24] we developed the Nystrom-type algorithm, which performs the discretization of IE (2) with the aid of specially tailored quadrature formulas of the interpolation type; this entails a guaranteed and quick convergence of our algorithm.

Once the surface current was found, the total scattering cross-section of the strip was computed as

$$\begin{aligned} W_{\rm sc}&=\frac{2}{\pi k}\int_0^{2\pi}|\Phi(\varphi)|^2{\rm d}\varphi,\quad \Phi(\varphi)\\ &=\frac{\kappa}{4}\sin\,\varphi\int_{-1}^{+1}w(t){\rm e}^{-{\rm i}\kappa(t+1)\cos\,\varphi}{\rm d}t, \end{aligned} \tag{3}$$

and the absorption cross-section as

$$W_{\rm abs}=\frac{d}{2}\frac{{\rm Re}\,Z}{Z_0}\int_{-1}^{+1}|w(t)|^2\,{\rm d}t. \tag{4}$$

The sum of these two quantities is the extinction cross-section (ECS), and the Optical Theorem tells that they obey the power conservation law,

$$W_{\rm sc}+W_{\rm abs}=-(4/k){\rm Re}\,\Phi(\beta+\pi). \tag{5}$$

In our computations, equation (5) was always satisfied with machine precision that served as an additional (in view of the guaranteed convergence) partial validation of the numerical solution.

3. Surface plasmon resonances

A stand-alone micro-size graphene strip illuminated by an H-polarized wave (figure 1(a)) demonstrates a sequence of resonances in the THz range (see section 3 of [23]). In figure 2(a), the normalized (by $2d$) extinction spectra for the wave incident under the angles $\beta=90\,^\circ$ and $45\,^\circ$ at a strip with the Kubo-model parameters $\tau=1$ ps, $\mu_{\rm c}=1$ eV are presented, and $T=300$ K and the width $d=50$ μm in free space with $\nu_{\rm host}=1$, calculated numerically using the Nystrom-type algorithm.

At the inclined incidence the number of observed SP resonances is larger than at the normal incidence, while in either case their peak values become smaller at higher frequencies. The most pronounced is the lowest-frequency resonance P_1 at the normal incidence, although its full width at half-maximum (FWHM) is the largest, which indicates the smallest value of the associated Q-factor.

For better insight into resonances, we show in figure 2(b) a map of a normalized ECS as a function of the frequency and the incidence angle β for the same strip. Only the resonances on the odd-index SP modes are excited at the normal incidence because of the symmetry of their natural fields with respect to the x-axis. In contrast, both the odd and even-index resonances appear under the inclined incidence. Note that under the edge-on incidence ($\beta=0$) none of the resonances are excited due to the anti-symmetry of the SP-mode natural fields with respect to the y-axis, see below.

In figure 3, we present the in-resonance patterns of the total magnetic field in the near zone and of the scattered field in the far zone, at frequencies of 1.6 THz (a), 3.88 THz (b), and 5.49 THz (c) for $\nu_{\rm host}=1.4$ for a graphene strip of $d=50$ μm; the other parameters the same as in figure 2.

The SP resonances can be interpreted as one-dimensional (1D) Fabry–Perot resonances formed by the reflections of the SP natural wave of a graphene layer from the strip edges. Indeed, it is visible that in each resonance an odd number of half-wavelengths of the above-mentioned natural SP wave of a graphene sheet match the strip width, and the hotspots of the SP field are only seen at the strip faces. This is behaviour typical of the Fabry–Perot mechanism, which leads to the characteristic equation,

$${\rm exp}({\rm i}2\beta_a^{\rm SP}d+2\psi)=1, \tag{6}$$

where ψ is associated with the phase of the reflection coefficient of the SP wave from the strip edge (this value can be extracted from the fit of (8) to the actual resonance frequency

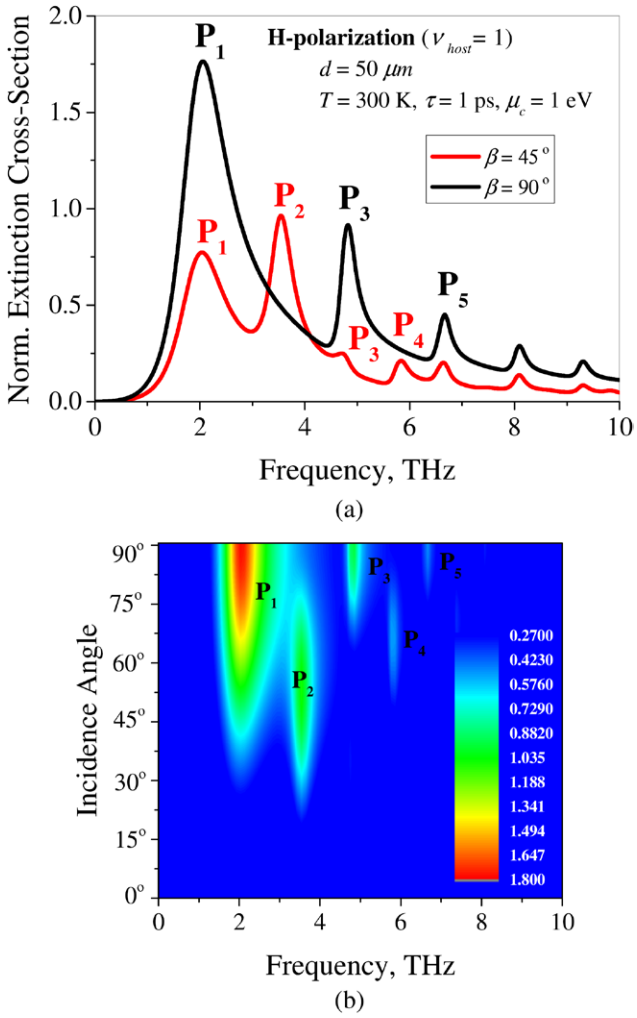

Figure 2. (a) Normalized ECS for the H-polarized plane wave incident normally at a stand-alone graphene strip as a function of the frequency; (b) color map of the normalized ECS as a function of frequency and incidence angle for a graphene strip with a width $d = 50$ μm.

of the first-order mode, P_1), and β^{SP} is the complex-valued propagation constant of the SP wave.

The latter value can be obtained analytically using the resistive boundary condition (1) applied to the infinite sheet of graphene and, additionally, the demand of anti-symmetry on the magnetic field component H_z across the plane where the strip is located [20, 21] (note misprint in equation (14) of [21] where the power 2 should be corrected to -2). The result is

$$\beta^{SP} = k[1 - 4(Z/Z_0)^2]^{1/2}, \tag{7}$$

where $k = k_0\nu_{host}$ ($k_0 = \omega/c = 2\pi/\lambda$). Equation (6) is satisfied if

$$\mathrm{Re}\,[\beta^{SP}(\lambda)]d = m\pi - \psi. \tag{8}$$

Then the corresponding natural frequencies of the P_m modes are associated with the odd-index roots ($m = 1, 3, 5, ...$) of (8) or the even-index roots ($m = 2, 4, ...$), respectively.

3.1. Bulk refractive-index sensitivities and figures-of-merit

In the design of optical or THz-range sensors, two values characterizing their performance are met: The sensitivity and the FOM [13–15].

By definition, the bulk refractive-index sensitivity $S_m^{bulk} = \Delta\lambda_m/\Delta\nu_{host}$ of the optical resonance of the mth order is given by the resonance wavelength shift $\Delta\lambda_m$ obtained under the refractive index variation $\Delta\nu_{host}$. The FOM is defined as $FOM_m = S_m^{bulk}(FWHM)^{-1}$, see [13–15]. Both values can be obtained numerically, after computing the ECS dependencies on the wavelength and the host-medium refractive index. Note that finding the FWHM values requires the use of the Fano-shape fitting procedure applied to the ECS spectral dependence (see appendix B).

However, besides that, it is interesting that the SP-resonances sensitivities can be estimated analytically with the aid of expressions (7) and (8), this was first noticed in [25]. We tried to derive more accurate expressions using the Kubo formula (A.2) instead of a simplified Drude formula used in [25]. Then the resonance wavelength of the mth SP mode is obtained as

$$\lambda_m = \frac{2d\nu_{host}}{m - c_1}\mathrm{Re}\sqrt{1 - 4(Z/Z_0)^2}, \tag{9}$$

where we denoted $c_1 = \psi/\pi$. Now, one should keep in mind that the impedance Z is a function of the frequency and can be approximated in the following way by using the formulas (A.1)–(A.3) and taking into account only the intraband transitions because of the small losses:

$$Z(\omega_m) \approx -\mathrm{i}\frac{c_2}{\lambda_m}, \quad c_2 = \frac{2\pi^2\hbar^2 c}{q_e^2 k_B T}\left[\frac{\mu_c}{k_B T} + 2\ln(1 + \mathrm{e}^{-\mu_c/k_B T})\right] > 0. \tag{10}$$

This brings us to the following formula:

$$\lambda_m = 2\left(\frac{\nu_{host}dc_2}{m - c_1}\right)^{1/2}. \tag{11}$$

Then, respectively, the sensitivity is

$$S_m^{bulk} = \frac{\partial\lambda_m}{\partial\nu_{host}} = \frac{1}{\sqrt{\nu_{host}}}\sqrt{\frac{dc_2}{m - c_1}} = \frac{\lambda_m}{2\nu_{host}}, \tag{12}$$

where with good enough accuracy one can take $c_1 = 0$. Note that the last term in (12) looks exactly like the corresponding equation (7) in [25], although the resonance wavelength (11) is different from (6) of [25] because we used the Kubo formula. From (12), one can see that the sensitivity of any SP mode is larger for smaller values of the host-medium refractive index. This circumstance makes chemo-sensing applications (such as hydrogen detection) especially promising.

Further, as one of the definitions of the quality factor is $Q_m = \lambda_m/FWHM_m$ (besides the more usual $Q_m = -\mathrm{Re}\,\omega_m/2\mathrm{Im}\,\omega_m$). Then the FOM can be obtained as

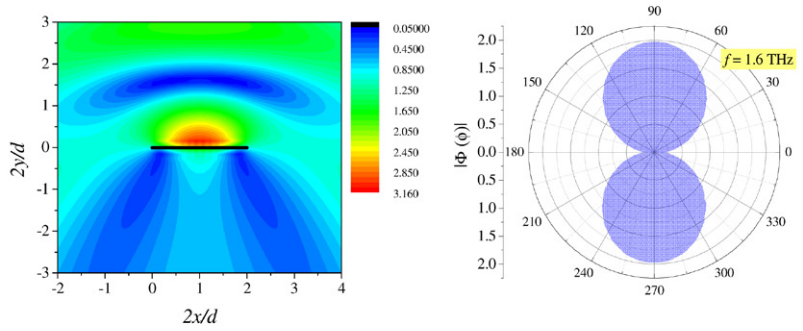

(a)

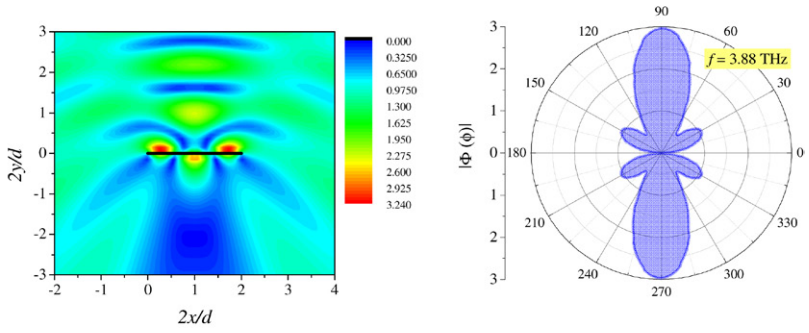

(b)

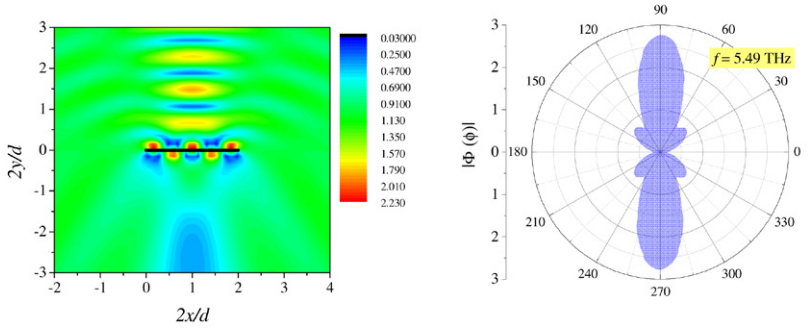

(c)

Figure 3. In-resonance total magnetic near-field patterns and scattered far-field diagrams for a graphene strip at frequencies 1.6 THz (a), 3.88 THz (b), and 5.49 THz (c) for $\nu_{\text{host}} = 1.4$ normal incidence. (a) P_1 resonance, (b) P_3 resonance, (c) P_5 resonance.

$$\text{FOM}_{\text{m}} = \frac{S_{\text{m}}^{\text{bulk}}}{\text{FWHM}_{\text{m}}} = \frac{1}{2} S_{\text{m}} Q_{\text{m}} \left(\frac{m - c_1}{\nu_{\text{host}} d c_2} \right)^{1/2} = \frac{Q_{\text{m}}}{2\nu_{\text{host}}}. \quad (13)$$

Although analytical expressions for the SP-mode quality factors Q_{m} are not available, they can be found, as previously mentioned, from the Fano fitting procedure; this can be called a semi-analytical evaluation.

As is visible from figures 2(a) and 4(a), all the resonances of ECSs are asymmetric Fano-shape (double-spike) resonances. This complicates the quantification of the linewidth of each of them. As a remedy, the extinction spectrum can be fitted with an analytical Fano formula [34] (see appendix B). The Fano fitting parameters for $\nu_{\text{host}} = 1.4$ are presented in table 1 and the corresponding fitted curve is also shown in figure 4(a) as dots. Note that refractive index close to 1.4 corresponds to a typical biosensing scenario of the water solution of proteins [13, 14].

Table 1. Fano fitting parameters ($A_0 = 0.02$).

	f (THz)	$(2\pi)^{-1}\Gamma$ (THz)	α	A
P_1	1.6	1.05	2.7	0.21
P_3	3.86	0.3	3.88	0.2
P_5	5.47	0.28	−0.15	−1.1

Figure 4(a) shows the normalized (by $2d$) extinction spectra for the H-polarized plane wave incident normally at a stand-alone graphene strip ($\tau = 1$ ps, $\mu_{\text{c}} = 1$ eV and $T = 300$ K) with a width $d = 50$ μm for four different values of the refractive index of the host medium, ν_{host}, calculated numerically via the Nystrom-type algorithm of (solid curves), and the corresponding Fano fit for $\nu_{\text{host}} = 1.4$ (dotted curve). Being visible, with the growth of the refractive index the resonance peaks shift down in frequency.

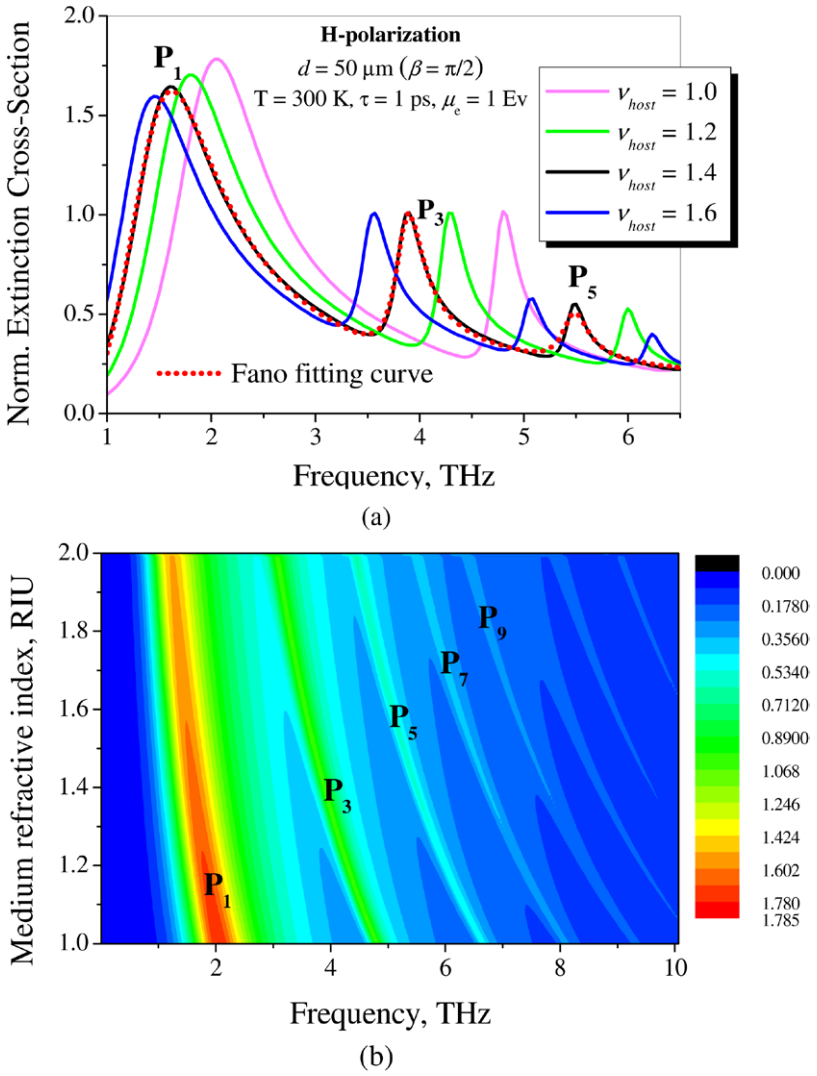

Figure 4. (a) Normalized ECS spectra of the graphene strip with a width $d = 50$ μm immersed in media with different refractive index values. (b) Map of the normalized ECS as a function of the frequency and medium refractive index. The normal incidence of the plane wave is assumed.

Table 2. Bulk sensitivity and FOM of the P_1, P_3, P_5 resonances.

	FWHM (μm) ($\nu_{\text{host}} = 1.4$)	$S_{\text{m}}^{\text{bulk}}$ (μm RIU^{-1}) (numeric.)	FOM (RIU^{-1}) (numeric.)	$S_{\text{m}}^{\text{bulk}}$ (μm RIU^{-1}) (analyt.)	FOM [RIU^{-1}] (semi-analyt.)
P_1	122.8	60.0	0.49	66.9	0.55
P_3	6.04	22.8	3.77	27.75	4.54
P_5	2.8	14.5	5.18	19.8	7.07

In figure 4(b) a map of the normalized ECS as a function of the frequency and medium refractive index is presented. This map along with the Fano fitting parameters enable us to find $S_{\text{m}}^{\text{bulk}}$ and FOM of the SP resonances numerically.

Comparative data on the three plasmon resonances are collected in table 2. We present here the values of the bulk sensitivity and FOM calculated in two ways; both numerically from the data in figure 4(b) along with the Fano fitting procedure; and analytically using the Kubo formula and expression (12) (for bulk sensitivity) or semi-analytically using the Kubo formulas and Fano fitting procedure (for the FOM). As can be seen, the sensitivity and FOM values obtained analytically and semi-analytically are 10 to 20% higher than their numerical counterparts. Besides, the highest bulk sensitivity is 60 μm RIU^{-1} for the P_1 resonance, although the FOM of the P_5 resonance, 5.18 RIU^{-1}, is more than 10 times larger than the FOM of the P_1 resonance, 0.49 RIU^{-1}.

This is apparently because of the higher values of the Q-factors of the higher-order plasmon modes of the graphene strip in the THz range, which is conditioned by the larger number of the surface-current nulls along the strip width. These FOM values are quite comparable to the characteristics of noble-metal strip sensors in the optical range [13–15].

4. Conclusions

Potential use of a micro-size graphene strip as a SP-resonance based bulk refractive index sensor in the THz frequency range was studied using a sophisticated numerical treatment of the associated singular IEs. This study was focused on the bulk refractive-index sensitivities and FOM values of the associated plasmon resonances. The primary plasmon mode P_1 was found to be the most sensitive to the refractive-index changes among all the plasmon modes, although its FOM value was the lowest. Higher-order SP resonances displayed much higher FOM values explained by the higher Q-factors. These FOM values are approximately the same as for the localized SP resonances on the noble-metal strip in the optical range.

Appendix A. Graphene conductivity

Graphene conductivity is characterized applying the Kubo formula [1, 2, 28],

$$\sigma(\omega,\mu_c,\tau,T)=\sigma_{\rm intra}(\omega,\mu_c,\ \tau,T)+\sigma_{\rm inter}(\omega,\mu_c,\tau,T), \quad \text{(A.1)}$$

$$\sigma_{\rm intra}=\frac{iq_e^2k_BT}{\pi\hbar^2(\omega+i\tau^{-1})}\left(\frac{\mu_c}{k_BT}+2\ln\left[1+\exp\left(-\frac{\mu_c}{k_BT}\right)\right]\right) \quad \text{(A.2)}$$

$$\sigma_{\rm inter}=\frac{iq_e^2(\omega+i\tau^{-1})}{\pi\hbar^2}\int_0^\infty\left(\frac{\partial f_d(-E)-\partial f_d(E)}{(\omega+i\tau^{-1})^2-4(E/\hbar)^2}\right)\partial E,$$

$$f_d(E)=\left[\exp\left(\frac{E-\mu_c}{k_BT}\right)+1\right]^{-1}, \quad \text{(A.3)}$$

where $f_d(E)$ is the Fermi–Dirac distribution, $E=\omega\hbar$ is the energy, q_e is the elementary charge, $\hbar$ is the reduced Planck's constant, and k_B is the Boltzmann constant. The first term in (A.1) relates to the intraband contributions of graphene, which usually dominate in the low THz range, and the second term relates to the interband contributions of graphene, which become more important at higher frequencies. It should be noted that the interband conductivity $\sigma_{\rm inter}$ can be approximated by the following simpler formula under conditions $k_BT\ll|\mu_c|$ [29]:

$$\sigma_{\rm inter}\simeq\frac{iq_e^2k_BT}{4\pi\hbar^2}\left(\frac{2|\mu_c|-(\omega+i\tau^{-1})\hbar}{2|\mu_c|+(\omega+i\tau^{-1})\hbar}\right). \quad \text{(A.4)}$$

Analysis shows (see the plots in figure 1(b)) that graphene behaves almost like a frequency-independent resistor, with a significant purely inductive reactance. It is observed that an increase in the chemical potential μ_c leads to lower losses and an up-shift of frequencies, where graphene displays more inductive behavior. The latter feature makes this material appropriate for the propagation of complex SP waves, which are the transverse magnetic waves traveling along the sheet of graphene.

Appendix B. Fano fitting model

In contrast to classical Lorentzian resonances, the Fano resonance exhibits a distinctly asymmetric spectrum shape. As found by Fano, it can be fitted with the analytical formula [33],

$$W_{\rm ext}(\omega)=A_0+\sum_j A_j\frac{(\alpha_j\Gamma_j/2+\omega-\omega_j)^2}{(\omega-\omega_j)^2+(\Gamma_j/2)^2}, \quad \text{(B.1)}$$

where ω_j is the frequency, Γ_j describes the linewidth of the resonant peak (or FWHM of the corresponding resonance), α_j is the phenomenological shape parameter (or Fano asymmetry parameter), and A_0, A_j are the fitting constant factors. Note that in these notations the quality factor of the jth mode is $Q_j=\omega_j/\Gamma_j$.

References

[1] Geim K and Novoselov K S 2007 The rise of graphene *Nat. Mater.* **6** 183–91

[2] Gusynin V P, Sharapov S G and Carbotte J P 2007 Magnetooptical conductivity in graphene *J. Phys.: Condens. Matter* **19** 026222

[3] Jablan M, Buljan H and Soljacic M 2009 Plasmonics in graphene at infrared frequencies *Phys. Rev.* B **80** 245435

[4] Otsuji T, Boubanga Tombet S A, Satou A, Fukidome H, Suemitsu M, Sano E, Popov V, Ryzhii M and Ryzhii V 2012 Graphene-based devices in terahertz science and technology *J. Phys. D: Appl. Phys.* **45** 303001/9

[5] Vakil A and Engheta N 2012 Transformation optics using graphene *Science* **332** 1291–4

[6] Chen P Y and Alu A 2011 Atomically thin surface cloak using graphene monolayers *ACS Nano* **5** 5855–63

[7] Filter R, Farhat M, Steglich M, Alaee R, Rockstuhl C and Lederer F 2013 Tunable graphene antennas for selective enhancement of THz-emission *Opt. Express* **21** 3737–45

[8] Fallahi A and Perruisseau-Carrier J 2012 Design of tunable biperiodic graphene metasurfaces *Phys. Rev.* B **86** 195408/9

[9] Jha K R and Singh G 2013 Terahertz planar antennas for future wireless communication: a technical review Infrared *Phys. Technol.* **60** 71–80

[10] Yu R, Alaee R, Lederer F and Rockstuhl C 2014 Manipulating the interaction between localized and delocalized surface plasmon-polaritons in graphene *Phys. Rev.* B **90** 085409

[11] Xu Z, Dong X and Bornemann J 2014 Design of a reconfigurable MIMO system for THz communications based on graphene antennas *IEEE Trans. Terahertz Sci. Technol.* **4** 609–17

[12] Mason D R, Menabde S G and Park N 2014 Unusual Otto excitation dynamics and enhanced coupling of light to TE plasmons in graphene *Opt. Express* **22** 847–58

[13] Homola J 2008 Surface plasmon resonance sensors for detection of chemical and biological species *Chem. Rev.* **108** 462–93

[14] Offermans P, Schaafsma M C, Rodriguez S R K, Zhang Y, Crego-Calama M, Brongersma S H and Rivas J G 2011 Universal scaling of the figure of merit of plasmonic sensors *ACS Nano* **5** 5151–7

[15] Shapoval O V 2015 Comparison of refractive-index sensitivities of optical-mode resonances on a finite comb-like grating of silver nanostrips *IEEE J. Quant. Electron.* **51** 7200108

[16] Han M Y *et al* 2007 Energy band gap engineering of graphene nanoribbons *Phys. Rev. Lett.* **98** 206805

[17] Ricciardi A *et al* 2013 Surface vs. bulk sensitivity of sensors based on Rayleigh anomalies in metallic nanogratings *Proc. SPIE, Opt. Sens.* **8774** 87741V
[18] Du X, Skachko I, Barker A and Andrei E Y 2008 Approaching ballistic transport in suspended graphene *Nat. Nanotechnol.* **3** 491–5
[19] Low T and Avouris P 2014 Graphene plasmonics for terahertz to mid-infrared applications *ACS Nano* **8** 1086–101
[20] Nikitin A Y, Guinea F, García-Vidal F J and Martín-Moreno L 2011 Edge and waveguide terahertz surface plasmon modes in graphene microribbons *Phys. Rev.* B **84** 161407(R)
[21] Nikitin A Y, Guinea F, Garcia-Vidal F J and Martin-Moreno L 2012 Surface plasmon enhanced absorption and suppressed transmission in periodic arrays of graphene ribbons *Phys. Rev.* B **85** 081405(R)/4
[22] Thongrattanasiri S, Koppens F H L and Garcia de Abajo F J 2012 Complete optical absorption in periodically patterned graphene *Phys. Rev. Lett.* **108** 047401/5
[23] Balaban M V, Shapoval O V and Nosich A I 2013 THz wave scattering by a graphene strip and a disk in the free space: integral equation analysis and surface plasmon resonances *J. Opt.* **15** 114007
[24] Shapoval O V, Gomez-Diaz J S, Perruisseau-Carrier J, Mosig J and Nosich A S 2013 Integral equation analysis of plane wave scattering by coplanar graphene-strip gratings in the THz range *IEEE Trans. Terahertz Sci. Technol.* **3** 666–73
[25] Vasić B, Isić G and Gajić R 2013 Localized surface plasmon resonance in graphene ribbon arrays for sensing of dielectric environment at infrared frequencies *J. Appl. Phys.* **113** 013110
[26] Hwang R-B 2014 Rigorous formulation of the scattering of plane waves by 2D graphene-based gratings: out-of-plane incidence *IEEE Trans. Antennas Propag.* **62** 4736–45
[27] Zinenko T L 2015 Scattering and absorption of terahertz waves by a free-standing infinite grating of graphene strips: analytical regularization analysis *IOP J. Opt.* **17** 055604
[28] Hanson G W 2008 Dyadic Green's functions for an anisotropic, non-local model of biased graphene *IEEE Trans. Antennas Propagat.* **56** 747–57
[29] Hanson G W 2008 Dyadic Green's functions and guided surface waves for a surface conductivity model of graphene *J. Appl. Phys.* **103** 064302
[30] Hall R C and Mittra R 1985 Scattering from a periodic array of resistive strips *IEEE Trans. Antennas Propag.* **33** 1009–11
[31] Volakis J L, Lin Y C and Anastassiou H 1994 TE characterization of resistive strip gratings on a dielectric slab using a single-mode expansion *IEEE Trans. Antennas Propag.* **42** 205–13
[32] Zinenko T L, Nosich A I and Okuno Y 1998 Plane wave scattering and absorption by resistive-strip and dielectric-strip periodic gratings *IEEE Trans. Antennas Propag.* **46** 1498–505
[33] Shapoval O V, Ctyroky J and Nosich A I 2013 Resonance effects in the optical antennas shaped as finite comb-like gratings of noble-metal nonstrips *Proc. SPIE* **8781** 87810U
[34] Fano U 1961 Effects of configuration interaction on intensities and phase shifts *Phys. Rev.* **124** 1866–78